Layer-resolved Magnetic Domain Imaging Using X-ray Photoelectron Emission Microscopy

W. KUCH, L.I. CHELARU, F. OFFI, M. KOTSUGI, X. GAO, K. FUKUMOTO AND J. KIRSCHNER
Max-Planck-Institut für Mikrostrukturphysik, Weinberg 2, D-06120 Halle, Germany

Basic and applied research on magnetic multi-layered structures has experienced an enormous increase in attention during the last decade. One of the main driving forces behind this progress was the commercial application of giant magnetoresistive effects in sensors and in hard disk read heads (1). Many other new and exciting phenomena, such as spin-polarized tunneling (2), spin-torque transfer (3,4), the prospect of assembling magnetic random access memory devices from nano-sized magnetoresistive elements (5), or the injection of spin-polarized electrons into semiconductors (6,7) have also caused a lot of excitement. All of these effects have in common the fact that the structures in which they are observed contain two or more magnetic layers within a multi-layered thin film structure, and that the magnetization of these layers has to be controlled independently. Since these samples are often laterally structured or confined, micromagnetic effects are becoming increasingly important. Its fundamental investigation requires a method that is not only capable of probing the magnetic properties of each magnetic layer separately, but also provides the necessary lateral resolution. Imaging with photoelectron emission microscopy (PEEM) in connection with X-ray magnetic circular dichroism (XMCD) in absorption (8) is such a method.

XMCD imaging with PEEM

In XMCD, the absorption of circularly polarized X-rays at elemental absorption edges depends on the relative orientation of the sample magnetization and the helicity of the exciting circularly polarized X-rays (9). For magnetic imaging with XMCD-PEEM, the secondary electron intensity distribution emitted from the sample surface is taken as a measure for the local X-ray absorption, which in turn depends on the local magnetization direction. These secondary electrons are used to create a magnified image of the sample surface by an electrostatic electron optics. The image intensity consequently depends on the local magnetization direction, projected onto the light incidence direction.

Figure 1 shows a schematic explanation of the method and the used instrument. The left side sketches the origin of the magnetic contrast. In a square microstructure, magnetic domains with four different magnetization directions yield different secondary electron intensity under irradiation with circularly polarized X-rays at resonance, as indicated by blue arrows. The magnified image (typical magnification 200–1000) displays the different domains with different image intensity. In practice, grayscale or color coded images of the asymmetry between two images acquired with opposite light helicity are presented. They are obtained by dividing the difference image by the sum image. Topological information thus cancels out in the asymmetry images.

The microscope (10), shown on the right side of Figure 1, is a straight axis electrostatic electron optics. Circularly polarized X-rays reach the sample surface under an angle of 30°. A high electric field, typically 10–15 kV/2 mm, accelerates the emitted electrons towards the objective lens, which creates an intermediate image in the plane of the field aperture. The contrast aperture, located in the back focal plane of the objective lens, limits the angular and energetic spread of the accepted electrons. Astigmatisms and misalignments of the optical axis can be corrected by an electrostatic octupole deflector/stigmator. The image is projected onto a double multichannel plate by two projective lenses, after intensification converted into visible light by a fluorescent screen, and computer recorded by a 12 bit CCD camera.

The images presented in the following have been obtained at the UE56/2 PGM-2 helical undulator plane grating beamline at BESSY

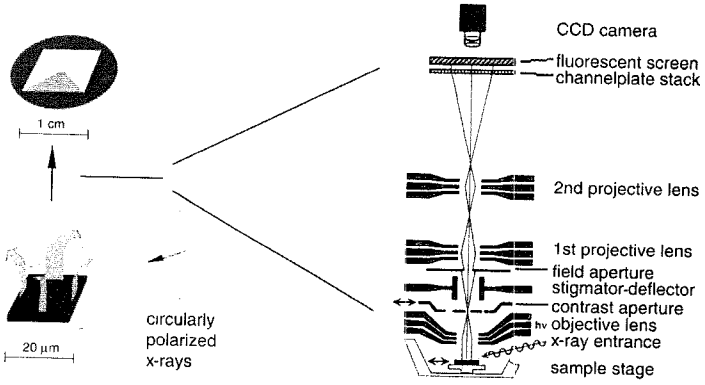

Figure 1: Schematic explanation of magnetic imaging with PEEM. Left: Due to XMCD, absorption of a microstructured sample consisting of four magnetic domains is locally different according to the domain structure. This leads to a locally different yield of photo-emitted electrons. A magnified image of the sample created from these electrons displays the magnetic information as intensity differences. Right: Sketch of the PEEM. Important components are three electrostatic lenses, a contrast aperture to limit the accepted range of electron emission angles, and an image converter consisting of a double multichannel plate and a fluorescent screen.

(Max-Planck-Society CRG beamline). Radiation from the fifth harmonic of the undulator was used, with a degree of circular polarization of about 80 percent (11). Epitaxial magnetic films and multilayers were prepared *in situ* in the ultra-high vacuum system with a base pressure of 10^{-8} Pa by electron beam assisted thermal evaporation onto a Cu(001) single crystal substrate held at room temperature. "As grown" domain images are presented in the following, i.e., obtained before exposing the samples to external magnetic fields. Extractor voltage and contrast aperture were set to 13 kV and 70 μm, respectively, resulting in a lateral resolution of about 350 nm.

Vectorial magnetic domain imaging

To obtain the full information about the magnetization vector of each domain seen in the sample, it is necessary to acquire images of the same spot of the sample for different light incidence angles. An example is shown in Figure 2. It presents domain images of a thin Ni film, deposited on Cu(001) as a 0–20 atomic monolayers (ML) thick wedge of 75 μm width, and capped by 11 ML Cu (12). The sample structure is schematically explained at the bottom of Figure 2. The Ni thickness increases in the images from bottom to top, as indicated at the left axes. The images show the magnetic domains in the Ni wedge, obtained from the XMCD contrast at the Ni L_3 absorption edge (851 eV photon energy). Two images for different azimuthal orientations of the light incidence, indicated by arrows labeled "$h\nu$", have been obtained by rotating the sample about its surface normal and re-adjusting the lateral position in order to keep the same field of view. The two images represent thus two independent measures of the local magnetization direction projection at each point of the image, which suffice to determine the two degrees of freedom of the magnetization direction in angular space. Comparing the two images, it is easy to distinguish magnetization directions parallel to the film plane ("in-plane") and magnetization directions along the surface normal ("out-of-plane"). The former undergo approximately a contrast reversal upon the near-180° change in X-ray incidence azimuth presented in Figure 2. The asymmetry contrast of the latter, on the other hand, does not change, since the light polarization component perpendicular to the film plane does not change.

Looking at the images of Figure 2, one recognizes a large region with out-of-plane magnetization for Ni thicknesses between 10 and 16 ML, characterized by a stripe-like domain pattern. At Ni thicknesses between 8 and 10 ML, as well as above 18 ML, the magnetization is in the film plane. The local magnetization directions are indicated in the images in some representative domains. There is a characteristic change in the stripe domain pattern as a function of Ni thickness in the out-of-plane region. Starting at about 14 ML Ni thickness, an increase in the number of stripes is recognized, which is accomplished by bifurcations in the stripe domains. This leads to a rapidly decreasing domain size. The shrinking of the average domain size is due to the competition between the magnetostatic energy and the energy cost for creating domains (13).

Layer-resolved magnetic domain images

The element-selectivity of the method makes it an ideal tool for the layer-resolved imaging of domains in more complicated layered structures, containing two or more magnetic layers. Figure 3 shows domain images of a Co/Cu/Ni trilayer, epitaxially grown on Cu(001), at low Co thicknesses and a constant Cu thickness of 4 atomic monolayers (ML) (14), as sketched at the top of the figure. The Co thickness increases from left to right, as indicated at the bottom axes. The images on the left show the domain pattern of the Ni layer, seen through the Co and Cu overlayers, obtained at the Ni L_3 edge. The images on the right show the domain pattern of the Co layer, obtained at the Co L_3 edge (778 eV photon energy). The top and bottom images show approximately the same position of the sample for different azimuth angles of the light incidence, as indicated by red arrows labeled "$h\nu$" As before, the magnetization vector in space can be determined from these two measurement geometries. Comparing the upper and lower images of Figure 3, it is seen that in the left part of the images, approximately below a Co thickness of 1.9 ML, the Co and Ni magnetizations are aligned in a collinear out-of-plane configuration. In the right part, the Co layer presents an

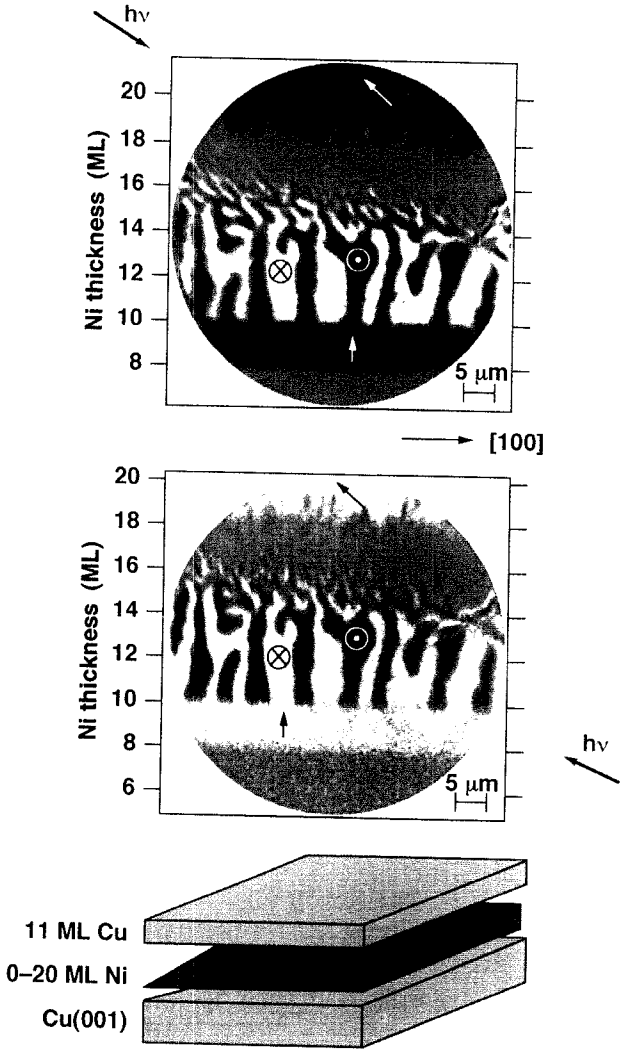

Figure 2: Magnetic domain images of a Cu/Ni double layer on Cu(001). The Ni layer was shaped into a micro-wedge, the thickness of which increases from bottom to top. The two images show the same region of the sample for different light incidence azimuth angles, as indicated by red arrows labeled "hν". This allows the distinction of in-plane and out-of-plane domains. The local magnetization direction is indicated in some domains. Two spin-reorientation transitions between in-plane and out-of-plane magnetization are observed as a function of Ni thickness, displayed at the left axes.

in-plane magnetization, as evidenced from the reversing contrast between the upper and lower Co images. In this region the Ni does show a change in contrast, but not a reversal as expected for in-plane magnetization. Here, consequently, the Ni magnetization is neither purely out-of-plane nor fully in-plane, but something in between. In the right part of the images, at Co thicknesses above ≈2 ML, a non-collinear magnetization configuration is thus present, in which the Co layer is magnetized in-plane, whereas the Ni layer is magnetized along canted axes (14). This canting can be understood considering the competition between the magnetic anisotropies of the Co and Ni layers and the magnetic interlayer coupling across the Cu spacer layer. Whereas the perpendicular anisotropy of the Ni layer tends to orient Ni out-of-plane, the interlayer coupling tries to align it parallel with the Co moment, thus leading to the canted configuration (15). For the very low Co thicknesses present in Figure 3, the Curie temperature of the Co layer is close to room temperature. The magnetic anisotropies are strongly reduced close to the Curie temperature, so that the Co layer is here easily rotated out-of-plane by the interlayer coupling.

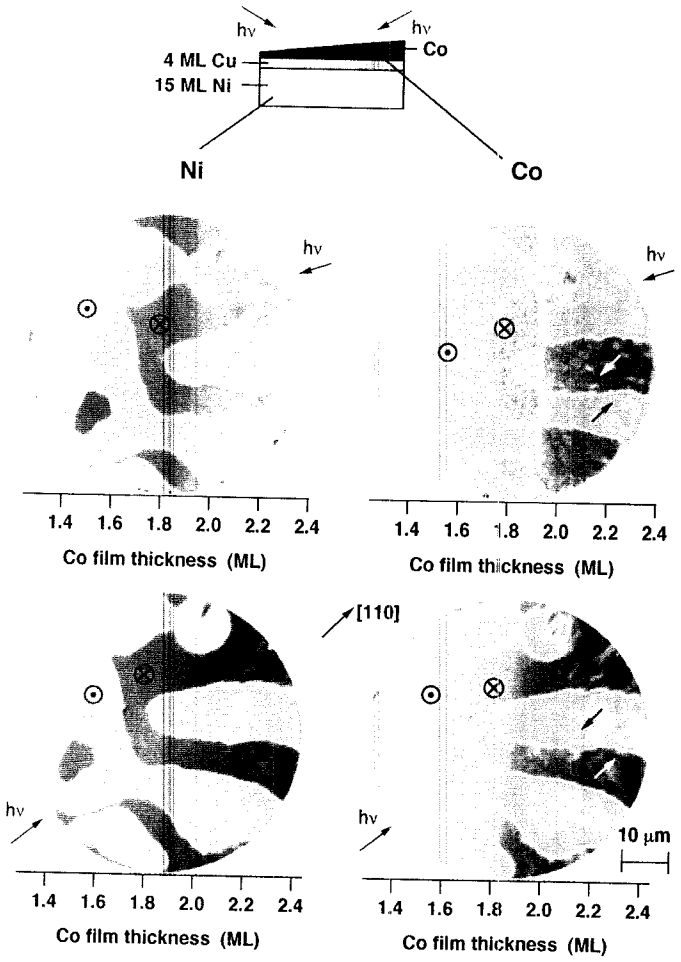

Figure 3: Layer-resolved magnetic domain images of a Co/Cu/Ni trilayer. The Co layer was shaped into a micro-wedge, the thickness of which increases from left to right. Domain images of the Ni bottom layer are shown on the left hand side, domain images of the Co top layer on the right hand side. Images obtained for different light incidence angles, as indicated by red arrows, are presented in the top and bottom line. At ≈2 ML Co thickness the magnetic configuration changes: In the left part of the imaged area Co and Ni magnetizations are collinearly aligned out-of-plane, whereas in the right part the Ni magnetization is at a canted non-collinear direction.

A set of layer-resolved domain images for a Co/Cu/Ni trilayer with higher Co and Cu layer thicknesses is shown in Figure 4. Here the sample was 4 ML Co/6 ML Cu/15 ML Ni/Cu(001). The image on the left shows the layer-resolved domain image of the Ni layer; the image on the right shows the domain image of the Co layer at the same sample position. Measurements under different geometries confirmed that due to magnetic anisotropies for this Cu spacer layer thickness the magnetization direction in the Ni layer was out-of-plane and the magnetization direction in the Co layer was in-plane, mainly along ±[110] crystallographic directions, as indicated in the sketch at the top of Figure 4. The Ni layer exhibits the typical stripe domain pattern of perpendicularly magnetized thin films. Although the Co magnetization, from an energetic point of view, does not need to follow the Ni magnetization in this non-collinear magnetization configuration, there is a certain correlation in the domain pattern of the out-of-plane magnetized Ni layer and the in-plane magnetized Co layer. The Co domains are arranged in lines that follow the stripe domains of the Ni layer. The mechanism that is leading to this correlation between Ni out-of-plane and Co in-plane domains on a lengthscale of micrometers is not yet fully clear. Micromagnetic interactions, for example between magnetostatic stray fields of domain walls, may play an important role. The detailed analysis of such meas-

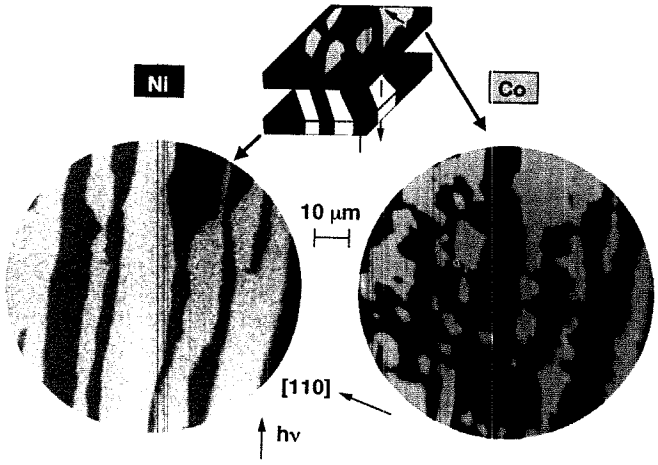

Figure 4: Layer-resolved magnetic domain images of a Co/Cu/Ni trilayer with 6 ML Cu spacer layer thickness. The domain image of the Ni layer is shown on the left, the domain image of the Co layer on the right. At that thickness the magnetization of the Ni layer is out-of-plane, whereas the Co magnetization is in-plane, as indicated in the sketch at the top of the figure. The Cu spacer layer has been omitted in the sketch for clarity. A correlation between the Ni and Co domain patterns is present, despite the mutually orthogonal magnetization directions.

urements is an ongoing project. It is expected to significantly further our understanding of the coupling mechanisms between ultrathin magnetic films including micromagnetic mechanisms, a subject that is at the leading edge of current magnetic thin film research.

In conclusion, layer-resolved magnetic domain imaging by XMCD-PEEM is an ideally suited tool for the study of magnetic interlayer coupling phenomena on short lengthscales. It combines lateral resolution and tunable sensitivity to different magnetic layers containing different elements, necessary ingredients for a successful exploration of the micromagnetic behavior of small magnetoresistive elements as they become smaller. ■

Acknowledgments

We would like to acknowledge the expert technical assistance of B. Zada and W. Mahler, and thank the BESSY staff for help and continuing support during the beamtimes. This work is supported by the German Federal Minister of Education and Science (BMBF) under Contract No. 05 KS1EFA6.

References

1. C. H. Tsang, J. R. E. Fontana, T. Lin, D. E. Heim, B. A. Gurney and M. L. Williams, *IBM J. Res. Develop.* **42,** 103 (1998).
2. J. S. Moodera and G. Mathon, *J. Magn. Magn. Mater.* **200,** 248 (1999).
3. E. B. Myers, D. C. Ralph, J. A. Katine, R. N. Louie and R. A. Buhrman, *Science* **285,** 867 (1999).
4. W. Weber, S. Riesen and H. C. Siegmann, *Science* **291,** 1015 (2001).
5. J.-G. Zhu, Y. Zheng and G. A. Prinz, *J. Appl. Phys.* **87,** 6668 (2000).
6. Y. Ohno, D. K. Young, B. Beschoten, F. Matsukura, H. Ohno and D. D. Awschalom, *Nature* **402,** 790 (1999).
7. A. T. Hanbicki, B. T. Jonker, G. Itskos, G. Kioseoglou and A. Petrou, *Appl. Phys. Lett.* **80,** 1240 (2002).
8. J. Stöhr, Y. Wu, B. D. Hermsmeier, M. G. Samant, G. R. Harp, S. Koranda, D. Dunham and B. P. Tonner, *Science* **259,** 658 (1993).
9. H. Ebert, *Rep. Prog. Phys.* **59,** 1665 (1996).
10. Focus IS PEEM (Omicron).
11. M. R. Weiss, R. Follath, K. J. S. Sawhney, F. Senf, J. Bahrdt, W. Frentrup, A. Gaupp, S. Sasaki, M. Scheer, H.-C. Mertins, D. Abramsohn, F. Schäfers, W. Kuch and W. Mahler, *Nucl. Instr. and Meth. A* **467–468,** 449 (2001).
12. K. Fukumoto, H. Daimon, L. Chelaru, F. Offi, W. Kuch and J. Kirschner, *Surf. Sci.* **514,** 151 (2002).
13. M. Speckmann, H. P. Oepen and H. Ibach, *Phys. Rev. Lett.* **75,** 2035 (1995).
14. W. Kuch, J. Gilles, X. Gao and J. Kirschner, *J. Magn. Magn. Mater.* **242–245,** 1246 (2002).
15. W. Kuch, X. Gao and J. Kirschner, *Phys. Rev. B* **65,** 064406 (2002).